ELSEVIER

Modeling wall impaction of diesel sprays

M. Gavaises, * A. Theodorakakos, and G. Bergeles
National Technical University of Athens, Department of Mechanical Engineering, Laboratory of Aerodynamics, Athens, Greece

A model for diesel spray wall impaction is presented, which is assessed against experiments for a number of test cases, including normal or angled injection to a wall into a quiescent space or a cross-flowing gas at various gas pressures. New relationships are given for the velocities of the droplets rebounding from the wall. These relationships take into account the wall roughness and the possible break-up of the droplets during their impingement. The impingement model was incorporated in a spray model based on the stochastic particle technique (Dukowicz 1980) and accounts for the phenomena of droplet injection, break-up, collision and coalescence, turbulent dispersion, and evaporation. The spray model was incorporated in a recently developed three-dimensional (3-D) computational fluid dynamics (CFD) code that simulates the unsteady compressible flow of the gas in internal combustion engines by solving the full Navier–Stokes equations. It was found that the motion of the surrounding gas caused by the spray injection plays a minor role on the predicted results. The latter concern the wall spray radius and the wall spray height. The validity of the spray model is demonstrated through extensive comparisons with experiments over a wide range of gas conditions.

Keywords: diesel spray; wall impaction; modeling

Introduction

Diesel spray impingement onto cylinder walls is an important phenomenon affecting engine combustion efficiency and emissions. The deposition of liquid fuel on the wall was generally regarded as having negative effects on the formation of combustible mixture and also as being the main cause of the higher level of hydrocarbon emissions often seen in small, high-speed direct injection engines.

Because of its complexity, experimental studies on the issue of spray-wall interactions began only in recent years and are almost all conducted with high-speed photographic techniques and carried out in laboratory test rigs at room temperature (Kuniyoshi et al. 1980; Fujimoto et al. 1990; Mirza 1991). Until now, presentation of experimental results were mainly concentrated on the distribution pattern of the wall spray. Two recently published works (Arcoumanis and Chang, 1993, 1994) focused mainly on the spray characteristics and the heat transfer between the spray and a heated plate onto which the spray was impinging. In the present work, two fundamental parameters, the wall spray height and the wall spray radius were selected for assessment of the relevant prediction model. The wall spray radius is defined as the mean average distance in the wall direction between the point at which the spray axis crosses the wall onto which the spray impinges and the ten droplets farthest from that point after their impaction. The wall spray height is defined as the mean average distance in the normal-to-the-wall direction between the point at which the spray axis crosses the wall onto which the spray impinges and the ten droplets farthest from that point after their impaction.

The first attempt of numerical simulation of spray impingement was performed by Naber and Reitz (1988), who considered three alternative ways of tracking droplets after wall impingement (Stick model, Reflect model, and Jet model). These models were employed in the KIVA code (Amsden et al. 1989) and applied in cases involving diesel spray impaction, either normal or at an angle onto a wall placed at a distance from the injector inside a pressurized chamber at room temperature (Kuniyoshi, experimental conditions 1980). Of the three ways of droplet tracking after their impingement, the Jet model was found to produce the best results. However, in a separate study (Naber et al. 1988), the Jet model had to be modified so that the normal velocity component of the reflecting droplets was chosen randomly in the range 0–34% of the normal velocity component of the droplet just before its impaction on the wall. Alloca et al. (1990) also used this modified Jet model in their simulation of normal spray impaction onto a wall. However, it seems that the results were not in satisfactory agreement with many of the experimental results. Also, Shih and Assanis (1991), implemented a new wall film evaporation model in the KIVA code, using a modification of the Jet model for the calculation of the droplet impingement. Another attempt by Wang and Watkins (1993), who reported a new droplet–wall impaction model implemented in a two-phase computational fluid dynamics (CFD) code, has shown that the wall spray radius is generally well

* Present address: Imperial College, Mechanical Engineering Department, Exhibition Road, London SW7 2BX, England.

Address reprint requests to Prof. G. C. Bergeles, Department of Mechanical Engineering, National Technical University of Athens, P. O. Box 64070, 15773 Zografou, Greece.

Received 14 April 1994; accepted 26 October 1995

Int. J. Heat and Fluid Flow 17: 130–138, 1996

655 Avenue of the Americas, New York, NY 10010

0142-727X/96/$15.00
SSDI 0142-727X(95)00097-6

predicted, but the wall spray height is underpredicted for all the test cases examined. Naitoh and Takagi (1994) also developed an impingement model to predict the secondary atomization of the droplets impinging on the valve of the inlet port of a spark ignition engine. Their model is a modification of the TAB model (O'Rourke and Amsden 1987), but no results were presented for predictions of diesel sprays. In a similar work by Senda et al. (1994), a developed impingement model, which is mainly based on a previous work by Wachters and Westerling (1966), was used for the prediction of the secondary atomization of the droplets impinging on a wall, the liquid film formation, and the heat transfer between the wall film and the heated wall. The predicted results, concerning only the wall spray radius, although they are closer to the experimental ones than the results of previously developed models, are for only one case of injection and impinging conditions.

In the present paper, a new wall impaction model is presented. The performance of the model is studied in a variety of wall impaction cases including normal and angled spray impaction in quiescent or cross-flowing gas and under a variety of gas chamber pressures in room temperature. The wall onto which the spray impinges has the same temperature of both the surrounding gas and liquid droplets. Therefore, the evaporation model is not tested. The pressure of the surrounding gas is similar to the pressures existing in a diesel engine; whereas, the gas velocity (cross-flow velocity) is analogous to the swirl. The reliability of the model predicting experiments under conditions without impingement has already been assessed (Assanis et al. 1993).

General approach

The simulation of diesel sprays is based on the discrete droplet model (DDM), in which the spray is represented by a number of droplet parcels each of which contains a large number of identical droplets with exactly the same properties that do not interact with each other. After their injection, the fuel is atomized into a much greater number of droplets (of smaller size) attributable to the TAB model as modified by Assanis et al. (1993). Then the liquid droplets disperse and coalesce as they move through the surrounding air. The aerodynamic drag of the moving droplets is taken into account. In each computational time-step, the droplets are translated by solving their trajectory equation (Lagrangian approach for the liquid phase). Then their new velocity and radius are calculated by taking into account all the physical phenomena mentioned above. In cases where impaction takes place, the velocity (magnitude and direction) and the size of the rebounding droplets has to be modeled. Also, the model has to take into account the possible break-up of the droplets at the moment of their impaction, as well as the formation of a fuel film on the walls.

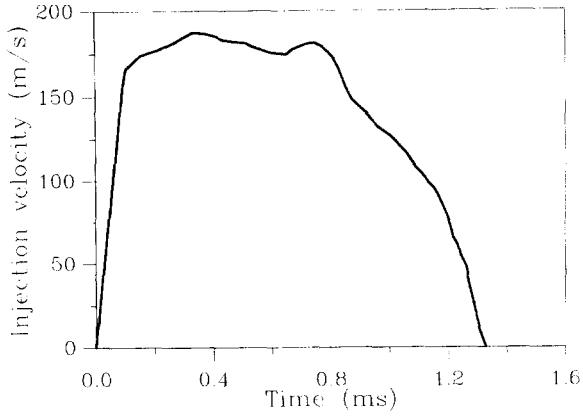

Figure 1 Variation of injection velocity with time for all test cases

In all cases studied, the duration of the injection was 1.33 ms, the injection nozzle diameter was 0.265 mm, and the flat disc, onto which the spray impinges, was located 0.032 m from the injector. Figure 1 shows the injection velocity profile for all the cases simulated, and Table 1 shows the various conditions for the experiments of Mirza (1991), which were simulated. It includes injection for three different gas pressures (6.9, 13.8, and 20.7 bar), three different cross-flow velocities (0.0, 9.4, and 13.5 m/s), and two different injection angles to the wall (0° and 30° to the vertical).

The effect of the spray injection on the motion of the surrounding gas was evaluated by taking into account the mass, momentum, and energy exchange between the liquid and the gas phase. The corresponding to that exchange coupling terms were added to a recently developed CFD code, which solves the full Navier–Stokes equation describing the compressible unsteady gas flow in complex geometries (i.e., inlet valve ports, internal combustion engines, etc). The time-averaged form of the continuity, momentum, and conservation equations for scalar variables were numerically solved using collocated Cartesian velocity components, on a Cartesian non-uniform numerical grid. Turbulence was simulated by the two equation $k-\varepsilon$ model. The discretization method was based on the finite volume approach, and the pressure correction method used is based on the SIMPLE algorithm. The spatial discretization scheme used was the hybrid scheme, and the temporal one was a first-order implicit Euler. The general form of these equations is given by Glekas and Bergeles (1993) and Demirdzic and Peric (1990). The general form of the coupling terms as well as their discrete form is given by Ramos (1989) or Amsden et al. (1989). It was found that the gas motion induced by spray injection has a minor effect on the

Notation

r	droplet radius
U	droplet velocity
We	Weber number
y	droplet surface displacement from its equilibrium position

Greek

α	angle of incidence
ΔE_{KLV}	loss of kinetic energy during droplet impingement
μ	droplet viscosity
ρ	density
σ	droplet surface tension
ψ	turn angle

Subscript

d	droplet
g	gas
in	just before the impingement
norm	normal
tang	tangential
out	just after the impingement

Table 1 Mirza's (1991) experimental conditions

Case	Gas pressure, bar	Injection angle, deg	Cross flow velocity, m/s
1	6.9	0	13.5
2	13.8	0	13.5
3	20.7	0	13.5
4	13.8	0	0.0
5	13.8	0	9.4
6	13.8	30	0.0
7	13.8	30	9.4
8	13.8	30	13.5

predicted wall spray radius and wall spray height. This happens because the ratio of the mass of the liquid fuel over the mass of the surrounding gas is very small for all the experimental conditions simulated and because there has been no evaporation of the liquid phase (injection at room temperature). Figures 2a and 2b show the predicted induced flow field for cases 4 and 5 of Table 1 (gas pressure 13.8 bar and cross-flow velocities 0.0 and 9.4 m/s, respectively) at time 1.2 ms after the start of the injection. A $45 \times 45 \times 35$ non-uniform numerical grid, covering a space of $10 \times 10 \times 3.2$ cm^3 has been used for the calculation of the gas motion. The computational time-step was $0.3 \cdot 10^{-5}$ s. These values for the time-step and the grid resolution were found to give time-independent, as well as grid-independent, results. The gas at the time of 1.2 ms after the start of the injection is expected to have its maximum velocity, because, as can be seen in Figure 1, at the time interval between 0.2 ms and 0.8 ms, the spray is injected with its maximum velocity, and the time needed until the spray impingement onto wall t_{imp} is approximately 0.4 ms for the test cases presented. It seems that the maximum induced gas velocity is approximately 30 m/s. As shown in Figure 2c, for the test case of gas pressure 13.8 bar and cross-flow velocity 9.4 m/s, the values of the wall spray radius and the wall spray height are in a range of 10% of their values calculated without taking into account the motion of the surrounding gas.

Modeling spray-wall impaction

In a discrete droplet spray model, it is preferred that the modeling of the droplet impingement on the walls be based on the fundamentals of individual droplets. According to Werlberger and Cartellieri's (1987) high-speed endoscopic photography observations, large droplets impinging on a wall form a liquid layer. On the other hand, Kuniyoshi et al. (1980), Katsuta et al. (1989), and Mirza's (1991) experiments demonstrate that small droplets are deflected away from the wall and taken away by the gas flow near the wall. Determining whether an approaching droplet forms a liquid layer on the wall or is reflected away from it depends on the droplet size, the wall temperature, material, roughness, the approaching angle and velocity of incident droplet, and other factors.

In a basic experimental study, Wachters and Westerling (1966) used single water drops of 1.7 mm diameter falling from a thin capillary tube onto an inclined hot polished metal surface at 400°C. Their objective was to determine the relationship between incident and rebounding velocities. It seems that some droplets, depending on the approaching Weber number, rebound from the wall, and others may break up into smaller ones after impinging on the surface.

Based on the above experimental observations, as a basic principle of droplet impingement modeling, we allow the impinging droplets either to rebound (with or without break-up) or to stick to the wall, depending on the Weber number, which is defined as $We = (2r_d \rho_d U_{norm}^2)/\sigma$ where ρ_d is the liquid density, U_{norm} is the normal to the wall droplet velocity component just before its impingement, r_d is the droplet radius, and σ is the droplet surface tension.

The model assumes that the droplet is reflected from the wall if its Weber number just before impaction is smaller than a critical value. Generally, no universal value for the critical Weber number exists, because different values have been proposed by various researchers. It should be also noted that the experimental conditions examined are not the same for all the experimental works (e.g., water sprays Wachters and Westerling 1966; diesel sprays Kuniyoshi et al. 1980). Also, the Weber number as a criterion for the wall film formation has been contested, because it does not take into account the liquid density and viscosity. In all cases, the formation of the wall film depends on the wall

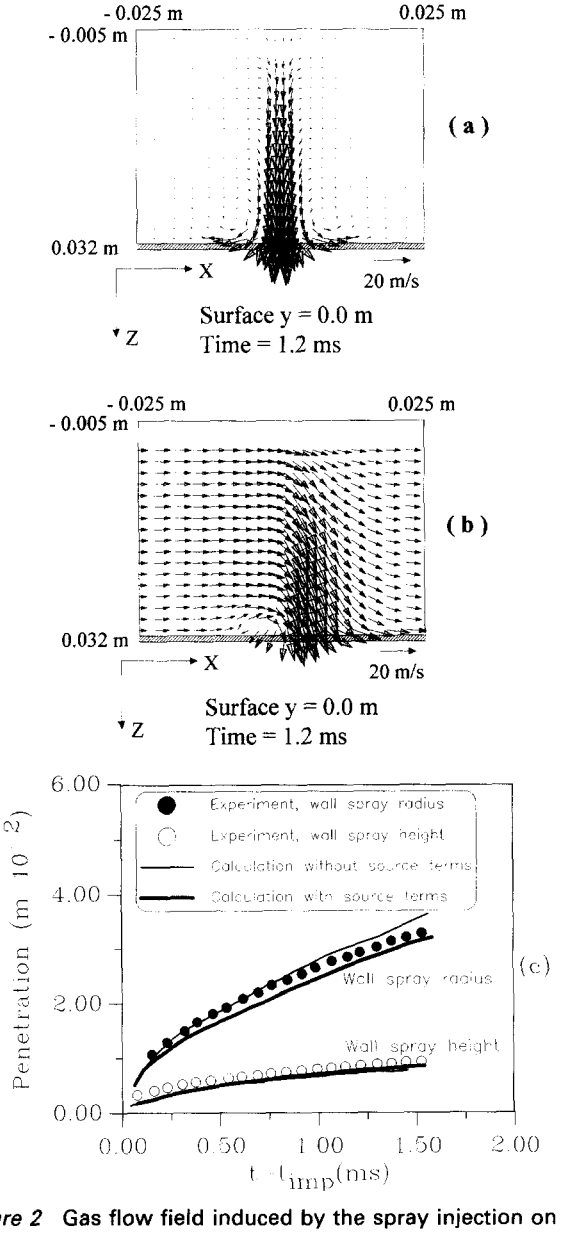

Figure 2 Gas flow field induced by the spray injection on the symmetry plane 1.2 ms after the start of injection (gas pressure 13.8 bar, normal injection): (a) cross-flow velocity 0.0 m/s; (b) cross-flow velocity 9.4 m/s; (c) effect of the gas motion induced by the spray injection on the predicted wall spray radius and wall spray height (cross flow 9.4 m/s)

temperature (Naber and Farrell 1993), the fuel properties, the gas pressure, and the injection conditions. Also, the flow field above the impinging wall affects the wall film evaporation rate and, as a consequence, its thickness. It the present study, the wall film thickness is assumed not to affect the velocities or the size of the rebounding droplets. Because of the differences on the widely accepted critical Weber number its effect on the predicted results was investigated. Figure 3a shows the calculated wall spray radius for four different values of the critical Weber number for case 4 (gas pressure 13.8 bar, cross-flow velocity 0.0 m/s). As

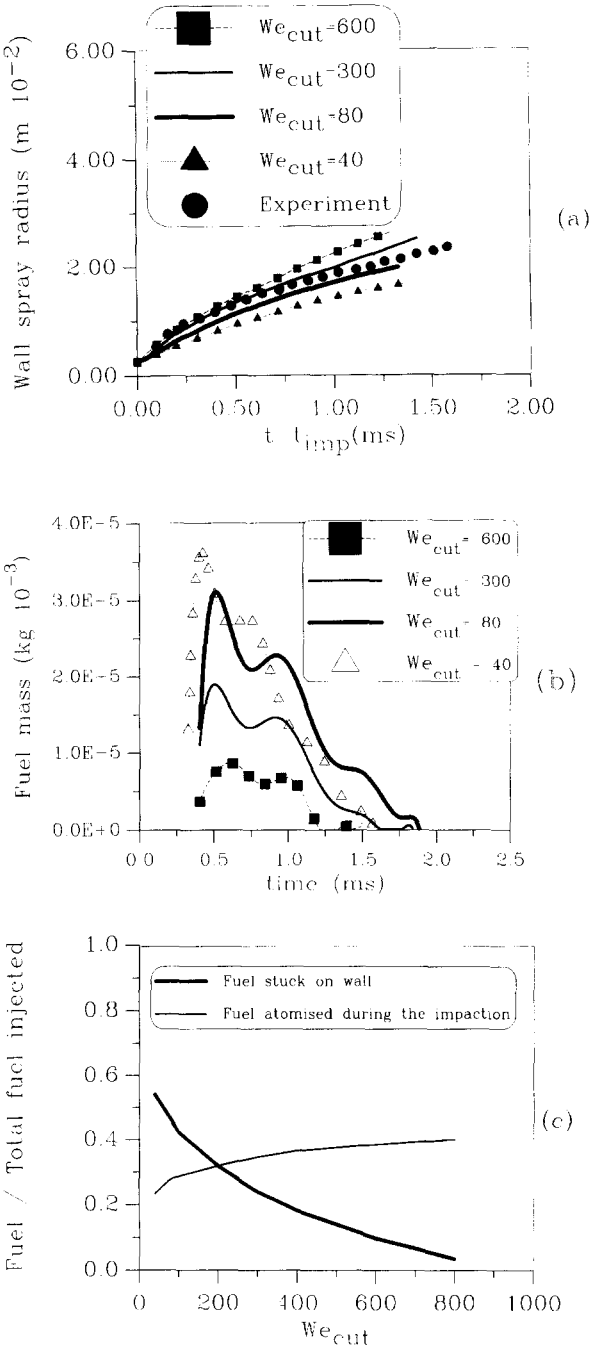

Figure 3 Effect of critical Weber number on (gas pressure 13.8 bar, cross-flow velocity 0.0 m/s, normal injection): (a) predicted wall spray radius; (b) fuel mass sticks on wall; (c) percentage total fuel sticks on wall and percentage total fuel atomized during spray impingement

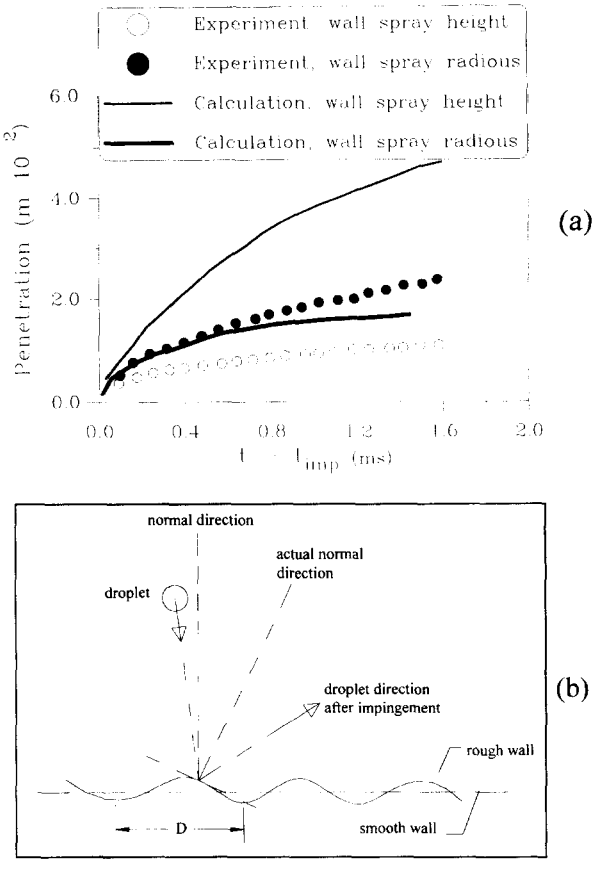

Figure 4 (a) Comparison between computational and experimental results for the wall spray radius and wall spray height using the reflect model (gas pressure 13.5 bar, cross-flow velocity 0.0 m/s, normal injection); (b) schematic representation of the wall roughness and of the angle of impaction

can be seen, for critical Weber numbers between 80 and 300, the variation of the wall spray radius is not significant; the effect on the wall spray height is even smaller. As can be seen from the Figure 3b, variation of the critical Weber number has a great effect on the amount of the fuel (per injection) that sticks on the wall. As expected, by increasing the value of the critical Weber number, the fuel that sticks on the wall decreases. Figure 3c shows the total fuel quantity that sticks on the wall divided with the total fuel injected. As can be seen, 46.3% of the total fuel injection quantity sticks on the wall for $We_{crit} = 80$, while 23.8% for $We_{crit} = 300$. Because no experimental data exist for the fuel that sticks on the wall and because the wall spray radius is slightly affected by the critical Weber number, the value selected for the simulation was $We_{crit} = 100$. This value is close to the value of $We_{crit} = 80$, which has been proposed by other researchers (Wang and Watkins 1993).

For determination of the droplet velocities after their impaction, the values of the wall spray radius and the wall spray height are plotted for case 4 (normal impaction, zero cross-flow velocity, and gas pressure 13.8) in Figure 4a, assuming that the droplets simply reflect from the wall with the magnitude of their tangential and normal-to-the-wall velocity components unchanged. It can be seen that the wall spray radius is smaller than the experimental one; whereas, the wall spray height is much higher (the normal-to-the-wall droplet velocities are much higher than the corresponding tangential one, because the spray is injected normal to the wall). That means that during their impaction, the droplets lose an amount of their kinetic energy. This

energy loss is mainly related to the normal-to-the-wall droplet velocity component, because the tangential one is a little smaller than that of the impinging droplet (because the experimental value of the wall spray radius is bit higher than the calculated one). A possible explanation of the difference in the tangential velocity component is presented schematically in Figure 4b (note that this figure is not to scale), where it can be seen that the actual normal-to-the-wall velocity component of the impinging droplet may differ from its value of a smooth wall, because the size of wall roughness D is the same order of magnitude as the size of the impinging droplets. The calculation of the normal-to-the-wall droplet velocity component after the impingement is based on the experimental results of Wachters and Westerling (1966). Their experimental data between the droplet Weber number just before and just after the impingement were found to fit to the correlation:

$$\mathrm{We}_{\mathrm{out}} = \min[\mathrm{We}_{\mathrm{in}}, \mathrm{Cimp}_1\mathrm{We}_{\mathrm{in}} \exp(-\mathrm{Cimp}_2\mathrm{We}_{\mathrm{in}})] \tag{1}$$

where $\mathrm{We}_{\mathrm{out}}$ and $\mathrm{We}_{\mathrm{in}}$ are the droplet Weber numbers after and before its impingement, respectively, and $\mathrm{Cimp}_1 = 0.687$, $\mathrm{Cimp}_2 = 0.04415$ are empirical constants. The value of Cimp_1 had to be modified in order to predict accurately the wall spray height. This assumption is valid, because their experiments concern water droplets with initial diameter 1.7 mm; these conditions are completely different from those found in diesel sprays. The value used for the simulation was $\mathrm{Cimp}_1 = 1.5$. Then, the normal-to-the-wall droplet velocity component can be calculated as follows:

$$U_{\mathrm{norm}}^{\mathrm{out}} = -U_{\mathrm{norm}}^{\mathrm{in}}\sqrt{\frac{d_{\mathrm{in}}\mathrm{We}_{\mathrm{out}}}{d_{\mathrm{out}}\mathrm{We}_{\mathrm{in}}}} \tag{2}$$

while, for the tangential one, the following relation is proposed:

$$U_{\mathrm{tang}}^{\mathrm{out}} = \mathrm{Cimp}_3\sqrt{\left(U_{\mathrm{norm}}^{\mathrm{in}}\right)^2 + \left(U_{\mathrm{tang}}^{\mathrm{in}}\right)^2 - \left(U_{\mathrm{norm}}^{\mathrm{out}}\right)^2} \tag{3}$$

where $U_{\mathrm{norm}}^{\mathrm{in}}$, $U_{\mathrm{tang}}^{\mathrm{in}}$, $U_{\mathrm{norm}}^{\mathrm{out}}$, $U_{\mathrm{tang}}^{\mathrm{out}}$ are the normal and the tangential-to-the-wall droplet velocity components of the impinging and the rebounding droplets, d_{in} and d_{out} are the droplets diameter just before and just after their impaction (the subscripts "norm" and "tang" stand for the normal and the tangential velocity components, respectively, while the superscripts "in" and "out" stand for the impinging and the rebounding droplets respectively), and Cimp_3 is a random number between (0, 1). With the second of the above equations, the value of the tangential component of the reflecting droplets may be smaller or greater than the value before its impaction. With this form, the wall roughness is statistically taken into account, because its actual value is not known, and no experimental data are available. Note also that in some cases, depending on the values of the above random number, the tangential component of the rebounding droplets may be much higher than the value of the normal one. To avoid any nonphysical result, we assume that the droplet will stick on the wall if arc tan $(U_{\mathrm{norm}}^{\mathrm{out}}/U_{\mathrm{tang}}^{\mathrm{out}}) < 1°$.

The calculation of the break-up of the droplets during their impingement (droplet secondary atomization) is also taken into account. As previously mentioned, for the calculation of the aerodynamic break-up of the droplets, the TAB model has been used. In this model, the droplet surface is assumed to be distorted and oscillating from its spherical scheme. The equation that describes the oscillation of the droplet surface from its initial undistorted position is the following:

$$\frac{\mathrm{d}^2y}{\mathrm{d}t^2} = \frac{c_f}{c_b}\frac{\rho_g}{\rho_d}\frac{u_{\mathrm{rel}}^2}{r_d^2} - \frac{c_k\sigma}{\rho_d r_d^3}y - \frac{c_d\mu_d}{\rho_d r_d^2}\frac{\mathrm{d}y}{\mathrm{d}t} \tag{4}$$

where y is the dimensionless displacement of the droplet surface from its equilibrium position [$y = x/(c_b r_d)$; x the displacement]; u_{rel} is the relative velocity between the droplet and the surrounding gas; ρ_d, σ, and μ_d are the density, surface tension, and viscosity of the droplet, respectively; r_d is the droplet radius; and c_f, c_k, c_b, and c_d are empirical constants. The droplet surface distortion during its impingement can be calculated by assuming that the energy of the surface distortion and oscillation is equal to the sum of its initial energy of surface distortion and oscillation and the loss of kinetic energy of the droplet during its impingement (so that there is no overall loss of energy). From this condition, and assuming that $(\mathrm{d}y/\mathrm{d}t)_{\mathrm{out}} = (\mathrm{d}y/\mathrm{d}t)_{\mathrm{in}}$ we can calculate the droplet distortion y during its impingement from the following relation:

$$(y_{\mathrm{out}})^2 = \frac{\frac{2}{3}\pi r_d^2 c_k\sigma y_{\mathrm{in}}^2 + \Delta E_{\mathrm{kin}}}{\frac{2}{3}\pi r_d^2 c_k\sigma} \tag{5}$$

where ΔE_{kin} is the loss of kinetic energy of the droplet during its impingement. Because the y of the rebounding droplet would be higher than that of the droplet just before its impaction, a possible break-up of the droplet may occur during the droplet impaction and reflection if the calculated value of the displacement y exceeds the critical value 1, which is required for the droplet to break-up. In Figure 3c the percentage fuel mass corresponding to the droplets that break up during the spray impingement is also plotted as a function of the critical Weber number. As can be seen, approximately 30% of the total fuel injected breaks up during the spray impingement for the previously selected value of the critical Weber number. The Sauter mean diameter (SMD) of the droplets after their secondary atomization can be estimated if we assume that the droplets are undistorted and not oscillating after their break up. The relation we get is

$$\mathrm{SMD} = \frac{4\pi\sigma}{\frac{4\pi\sigma}{r_d} + \frac{2\pi}{3}\rho_d r_d^2(\mathrm{d}y/\mathrm{d}t)_{\mathrm{in}}^2 + c_k\frac{\sigma}{\rho_d r_d^3}y_{\mathrm{in}}^2} \tag{6}$$

Figure 5 shows the effect of the droplet secondary atomization on the spray SMD. As can be seen, the SMD of the whole spray decreases by approximately 7 microns from its value calculated without secondary atomization. This value is approximately 20 microns, which is typical for diesel sprays. This value is also in agreement with the values of the SMD measured by Arcoumanis and Chang (1994) at spray impingement. It should be noted that, because the droplet diameter is involved to the calculation of $U_{\mathrm{norm}}^{\mathrm{out}}$, the droplet velocity components are recalculated from Equations 2 and 3.

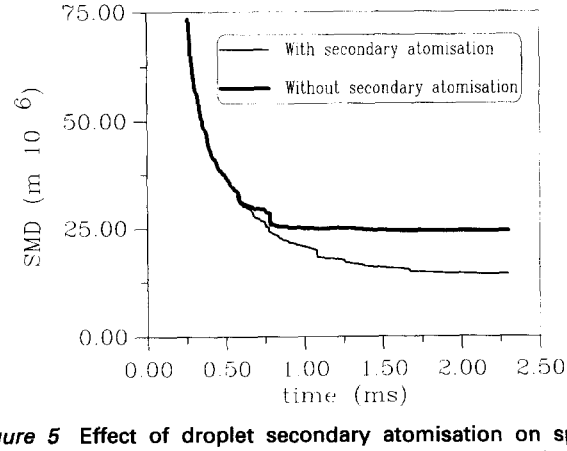

Figure 5 Effect of droplet secondary atomisation on spray SMD; gas pressure 13.8 bar, cross flow 0.0 m/s, normal injection

The determination of the direction of the tangential component of the reflected droplets is based on the experimental observation that the impinging droplets are reflected in different directions from their direction just before their impaction. The droplet may turn on the plane of the surface by an angle ψ with respect to the tangential velocity vector of the impinging droplet (Jet model, Naber and Reitz 1988). The turning angle ψ can be determined by a probability distribution function, derived assuming potential flow jet and conservation of mass and momentum. The turning angle ψ can be expressed as follows:

$$\psi = -\frac{\pi}{\beta}\ln\left[1-\chi(1-e^{-\beta})\right] \tag{7}$$

where χ is a random number between (0, 1), and β is a parameter determined from the relation

$$sin\ \alpha = \frac{e^{\beta}+1}{e^{\beta}-1}\frac{1}{1+(\chi/\beta)^2}$$

where α is the angle between the droplet velocity vector and the normal to the wall surface at the point of impingement.

Results and discussion

Initially, the reliability of the model is assessed through comparison between experimental and computational results for the wall spray radius and the wall spray height. Then, results for the SMD

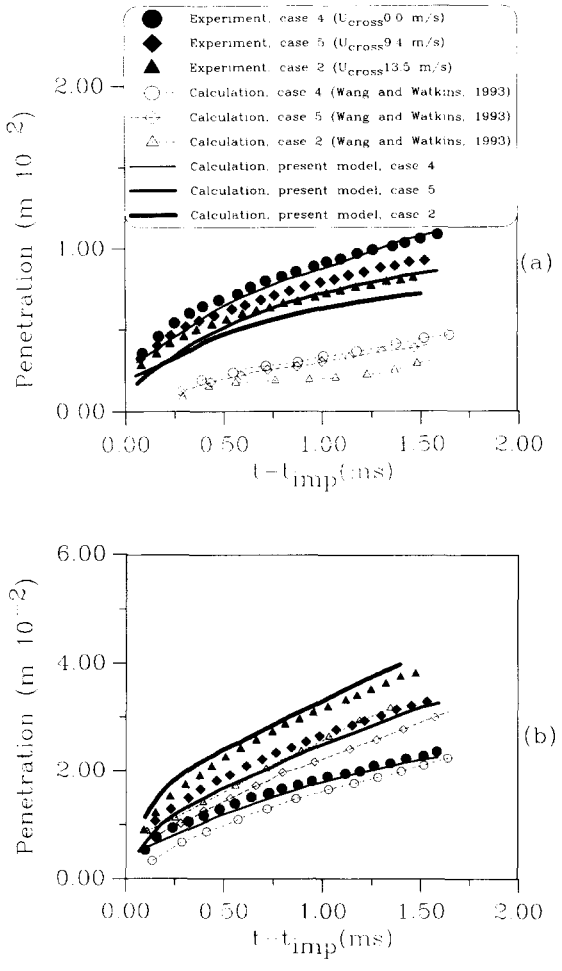

Figure 6 Effect of cross-flow velocity on (normal injection, gas pressure 13.8 bar): (a) wall spray height; (b) wall spray radius

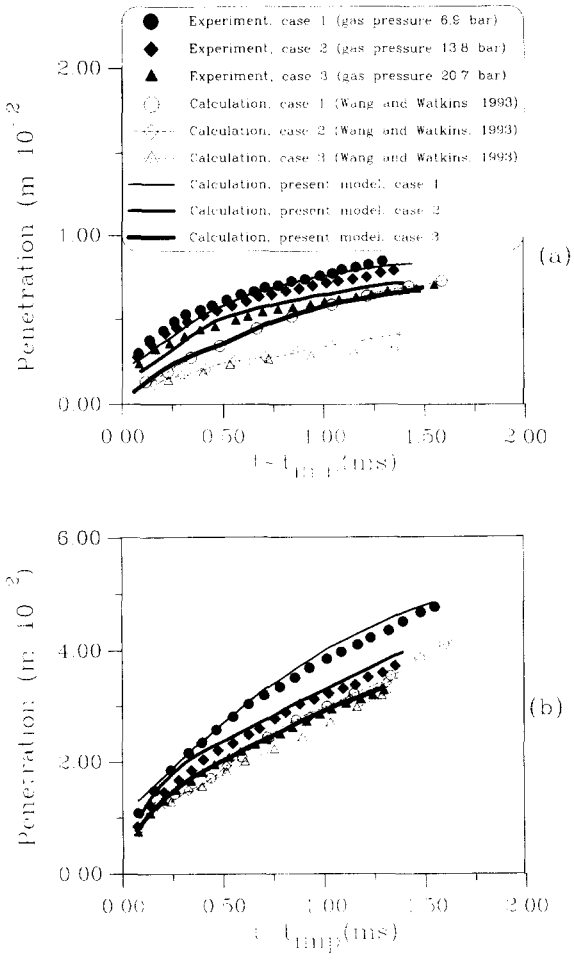

Figure 7 Effect of gas pressure on (normal injection, cross-flow velocity 13.5 m/s): (a) wall spray height; (b) wall spray radius

and the droplet velocities are presented, helping to understand qualitatively the impingement mechanism.

Figures 6a and 6b show the effect of the cross flow on the wall spray height and the wall spray radius, respectively, for constant gas pressure (13.8 bar) (cases 4, 5, and 2 of Table 1). As can be seen, by increasing the cross flow, the wall spray radius increases, but the wall spray height decreases. This happens because the gas sweeps the droplets along the direction of its motion. In the figures are also plotted the calculations of Wang and Watkins (1993). In the present model, both the wall spray radius and the wall spray height have been satisfactorily well predicted for all three cases. Particularly, the model seems to improve predictions especially for the wall spray height, which was substantially underestimated.

Figures 7a and 7b show the effect of gas pressure on the wall spray height and the wall spray radius, respectively, for the case of normal impaction and for 13.5 m/s cross-flow velocity (cases 1–3 of Table 1). Figure 9c shows pictorially the effect of gas pressure on the spray development (1.15 ms after the beginning of the injection). By increasing the gas pressure, both the wall spray height and the wall spray radius decrease. This is attributable to the increased droplet aerodynamic drag caused by the increase of the gas pressure. The conclusions drawn from the calculations are analogous to those of the previous Figures 6a and 6b. The wall spray height has been predicted with satisfactory accuracy; the slope of the curves is similar to the experimental one.

Figures 8a and 8b show the effect of cross-flow velocity on the wall spray height and the wall spray radius keeping the gas pressure constant (13.8 bar) and for angle of injection 30° from the vertical (cases 6–8 of Table 1). It can be seen that when the angle of injection increases, the wall spray radius increases considerably, because the droplets have a larger tangential velocity during their impingement.

A pictorial representation of the effect of the cross-flow velocity on the spray development can be seen by comparing Figures 9a and 9b. The pictures show the position of 800 representative computational parcels in the three-dimensional (3-D) space 1.15 ms after the start of the injection. In these figures the size of the "spheres" that represent the droplets, is proportional to their size. It can be clearly seen that the motion of the gas has great effect on the distribution of the droplets in space. Starting from the symmetrical distribution for zero cross-flow velocity, we proceed to increasingly inhomogeneous distribution as cross-flow velocity increases.

As a general conclusion from the assessment of the impinging model presented, it can be said that the model describes with satisfactory accuracy the scattering of the droplets following their impact on a flat disc for a wide range of gas pressures, angles of impact, and cross-flow velocities.

Furthermore, it would be useful to present some statistical results that will give a more complete view of the phenomenon because only a few measurements exist for the size and the velocities of the droplets during their impingement. Note that for

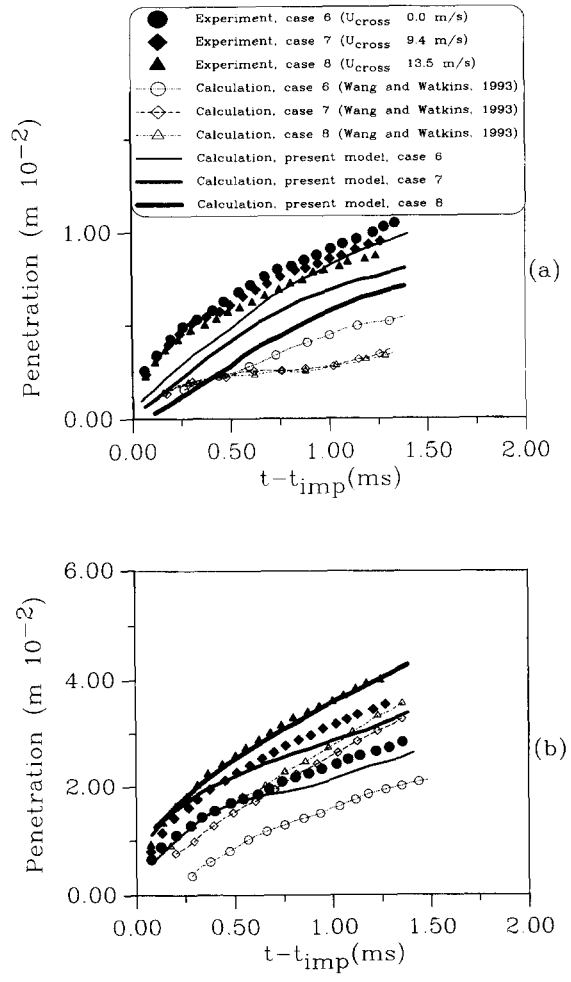

Figure 8 Effect of cross-flow velocity on (angled injection, gas pressure 13.8 bar): (a) wall spray height; (b) wall spray radius

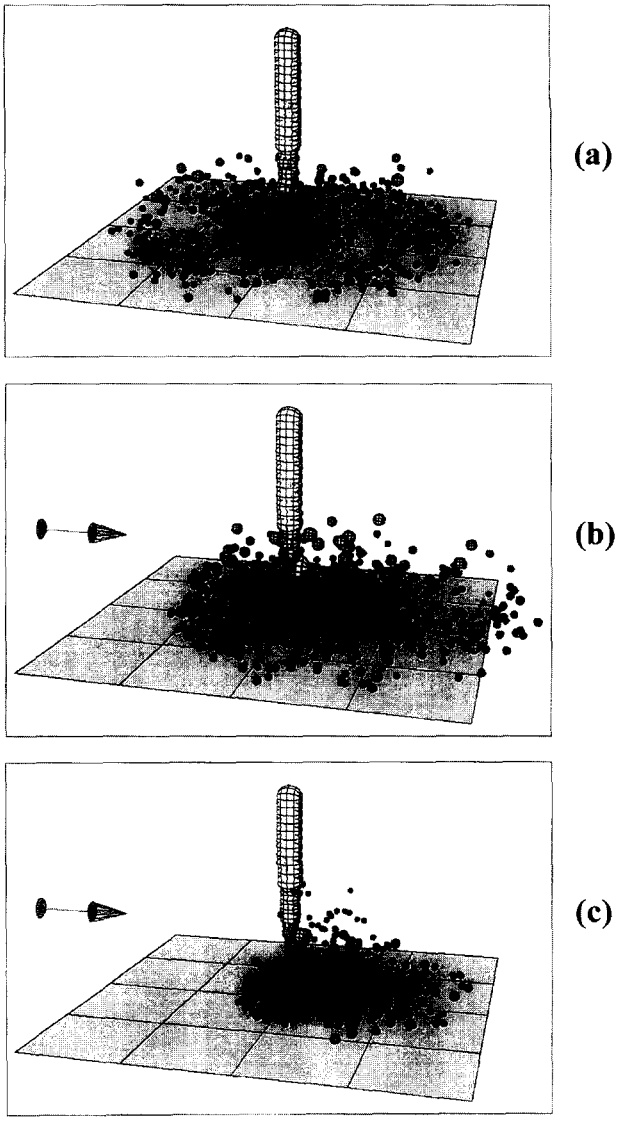

Figure 9 Effect of cross-flow velocity and gas pressure on spray development (normal impaction, time = 1.15 ms): (a) cross flow 0.0 m/s, gas pressure 13.8 bar; (b) cross flow 13.5 m/s, gas pressure 13.8 bar; (c) cross flow 13.5 m/s, gas pressure 20.5 bar

the statistical description of the aforementioned magnitudes, 100,000 droplet parcels have been used, enough to give statistically independent results.

Figures 10a and 10b show the temporal profiles of SMD on spray centerline 3.1 cm from the injector for case 4 of Table 1 (gas pressure 13.8 bar, zero cross-flow velocity). Figure 10a refers to the free spray, and Figure 10b has been obtained by placing the disc 0.032 m from the injector [similar to Mirza's (1991) experimental conditions] with the spray impinging normal on it. In Figure 10b the droplets cover a much larger space because of the spreading of the rebounding droplets (the lack of uniformity at the edges is caused by the small number of droplets existing far from the spray axis). As can be seen, although in the free spray the larger droplets are found in the center of the spray, the distribution of the SMD when the disc is placed lies closer to an off-center maximum distribution. It should be mentioned that the very large size of the droplets that seems to appear at the center of the spray does not represent the SMD value of all of the

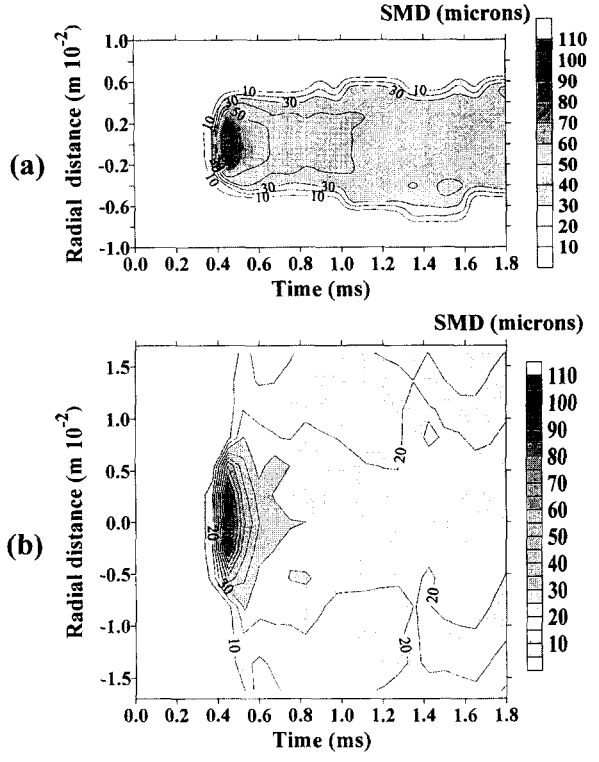

Figure 10 Effect of disc presence on the temporal profile of the centreline SMD (microns) 0.031 m from the injector (gas pressure 13.5 bar, cross-flow velocity 0.0 m/s): (a) free spray; (b) disc placed 0.032 m from the injector, normal impaction

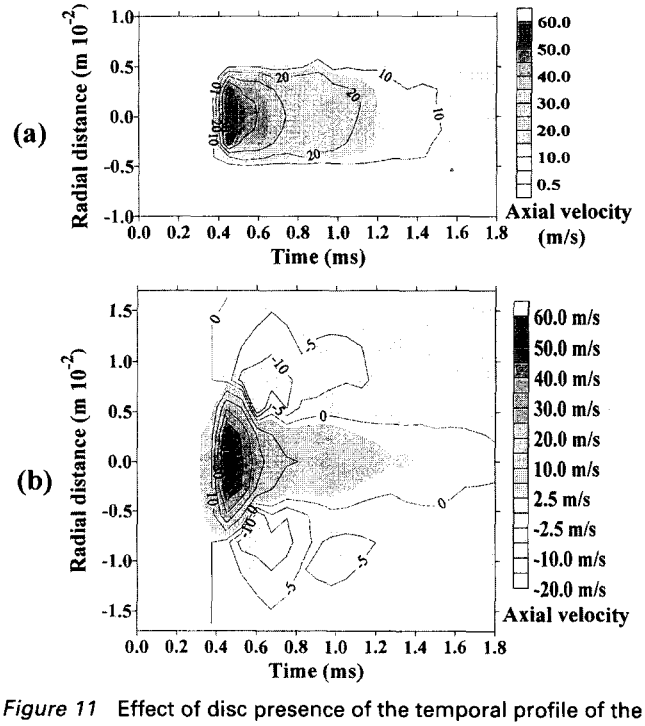

Figure 11 Effect of disc presence of the temporal profile of the centerline liquid mass mean axial velocity (m/s) 0.031 m from the injector (gas pressure 13.5 bar, cross-flow velocity 0.0 m/s): (a) free spray; (b) disc placed 0.032 m from the injector, normal impaction

spray droplets, which was presented in Figure 5. The large values that appear are related to the TAB break-up model. The diameter of the injected droplets is equal to the diameter of the injection hole of the nozzle from which they are injected. Larger droplets are found in the centerline of the free spray, because the smaller the size of the droplet, the higher the radial velocity component calculated from the model, and, thus, the higher the radial distance from the spray axis. It should be noted also that as the time increases, smaller droplets pass through the examined positions, because the SMD seems to decrease. Figures 11a and 11b show the liquid mass mean axial velocity distribution at the same positions and for the same gas conditions of Figure 10 for both a free spray and an impinging spray. The free spray velocity, which is approximately equal to the velocity that the spray impinges on the wall, decreases as the time increases. The maximum before impingement velocity is around 55 m/s at the time of 0.45 ms, while its value is around 20 m/s at time 1.0 ms after the beginning of the injection. As can be also seen, the spray velocity is higher at the spray axis and smaller at the edges. When the disc is placed, the maximum velocity of the rebounding droplets is approximately 15 m/s. Their velocity is much smaller, around 3 m/s away from the spray axis. It can be also seen that the mean spray velocity at the spray axis decreases, because rebounding droplets also exist at this location, although the most of the droplets found in that area have not impinged on the wall (note that the velocity presented refers to droplet mass and not to the number of the droplets).

Conclusions

A model of impaction of liquid droplets against a wall has been presented, based on the stochastic particle technique (Dukowicz 1980). The ability of the model to predict experimental results has been checked through comparison with experiments for a wide range of gas pressures, gas velocities, and angles of injection.

The effect of the gas motion caused by the spray injection on the wall spray radius and the wall spray height was estimated by solving simultaneously the gas and liquid phase equations. It was found that the spray is little affected by the induced gas motion.

The calculation of the velocities of the droplets rebounding from the wall was performed by new proposed relationships that take into account the kinetic energy losses of the droplets during their impingement and possible droplet break-up (secondary droplet atomization). From the total fuel injected, approximately 40% sticks on the wall during the droplets impingement, while 30% breaks up. From the comparison between the computational and the experimental results, it can be concluded that the impaction model describes the scattering of the droplets following their impact with satisfactory accuracy for most of the cases examined.

Information on the space and time distribution of the size of the droplets and their velocity has been given, enabling an understanding of the behavior of a spray impinging on a flat disc. It can be concluded that, in contrast to the free spray distributions, the SMD distribution exhibits a bimodal behaviour with maximum farther off the spray axis.

Acknowledgments

The authors would like to thank Mr M. Alexakis for his help in preparing the drawings on AutoCAD. Also, the authors would like to thank the reviewers of the paper for their comments and suggestions. This work was financially supported by the research contract JOUE CT91 0083.

References

Alloca, L., Amato, U., Bertoli, C. and Corcione, F. E. 1988. Comparison of models and experiments for diesel sprays, *Proc. Int. Symp. on Diagnostics and Modeling of Combustion in I.C.Engines*, 255–261, Kyoto, Japan

Amsden, A. A., O'Rourke, P. J. and Butler, T. D. 1989. KIVA-II: A computer program for chemically reactive flows with sprays. Los Alamos Report LA-11560-MS

Arcoumanis, C. and Chang, J-C. 1994. Flow and heat transfer characteristics of impinging transient diesel sprays. SAE Technical Paper Series 940678

Arcoumanis, C. and Chang, J-C. 1993. Heat transfer between a heated plate and a impinging transient diesel spray. *Exp. Fluids*, **16**, 105–119

Assanis, D., Gavaises, M. and Bergeles, G., 1993. Calibration and validation of the Taylor analogy break-up model for diesel spray calculations. *ASME, 93-ICE-11*, (January 31–February 4), Houston, TX

Demerdzic, I. and Peric, M. 1990. Finite volume method for prediction of fluid flow in arbitrary shaped domains with moving boundaries. *Int. J. Num. Meth. Fluids*, **10**, 771

Ducowicz, J. K. 1930. A particle–fluid numerical model for liquid sprays. *J. Comp. Phys.*, **35**, 229–233

Fujimoto, H., Senda, J., Nagae, M., Hashimoto, A., Saito, M. and Katsura, N. 1990. Characteristics of a diesel spray impinging on a flat wall. *Proc. Int. Symposium COMODIA 90*, 193–198

Glekas, J. P. and Bergeles, G. C. 1993. A numerical method for recalculating flows on generalized coordinates: Application in environmental flows. *Appl. Math. Model.*, **17**, 506

Katsura, N., Saito, N., Senda, M. and Fujimoto, H. 1989. Characteristics of a diesel spray impinging on a flat wall. SAE Technical Paper Series 890264

Kuniyoshi, H, Yamoto, H., Fujimoto, H. and Sato, G. T. 1980. Investigation of the characteristics of diesel fuel spray: Impinging upon a flat plate. *J. Mech. Eng. Soc. Japan*, **15**, 57–64

Mirza, R. 1991. Studies of diesel spray interacting with cross-flow and solid boundaries. Ph.D. thesis, Faculty of Technology, University of Manchester, UK

Naber, J. D., Enright, B. and Farrell, P. 1988. Modeling engine spray/wall impingement, SAE Paper 880107

Naber, J. D. and Farrell, P. V. 1993. Hydrodynamics of droplet impinging on a heated surface. SAE Technical Paper Series 930919

Naber, J. D. and Reitz, R. D. 1988. Modeling engine spray/wall impingement. SAE Paper 880107

Naitoh, K. and Takagi, Y. 1994. Oval-parabola trajectories (OPT) model of droplet — Wall interaction in engines. *Proc. Int. Symposium COMODIA 94*, 417–422

O'Rourke, P. J. and Amsden, A. A. 1987. The TAB method for numerical calculation of spray droplet break-up. SAE Paper 872089

Ramos, J. I. 1989. *Internal Combustion Engine Modeling*. Hemishere, Bristol, PA

Senda, J., Kobayashi, M., Iwashita, S. and Fujimoto, H. 1994. Modeling on diesel spray impinging on flat wall. *Proc. Int. Symposium COMODIA 94*, 411–416

Shih, K. and Assanis, D. N. 1991. Implementation of a fuel spray wall interaction model in KIVA-II. SAE Paper 911787

Wachters, L. H. J. and Westerling, N. A. J. 1966. The heat transfer from a hot wall to impinging water drops in the spherical state. *Chem. Eng. Sci.*, **21**, 1047–1065

Wang, D. M. and Watkins, A. P. 1993. Numerical modeling of diesel spray wall impaction phenomena. *Int. J. Heat Fluid Flow*, **14**

Werberger, P. and Cartellieri, W. P. 1987. Fuel injection and combustion phenomena in a high-speed DI diesel engine observed by means of endoscope high-speed photography. SAE Technical Paper Series 870097